Direct Evidence of Cation Disorder in Thermoelectric Lead Chalcogenides PbTe and PbS

*Sofie Kastbjerg, Niels Bindzus, Martin Søndergaard, Simon Johnsen, Nina Lock, Mogens Christensen, Masaki Takata, Mark A. Spackman, and Bo Brummerstedt Iversen**

The extraordinary thermoelectric properties of lead chalcogenides have attracted huge interest in part due to their unexpected low thermal conductivity. Here, it is shown that anharmonicity and large cation disorder are present in both PbTe and PbS, based on elaborate charge density visualization using synchrotron powder X-ray diffraction (SPXRD) data analyzed with the maximum entropy method (MEM). In both systems, the cation disorder increases with increasing temperature, whereas the Te/S anions appear to be centered on the expected lattice positions. Even at the lowest temperatures of 105 K, the lead ion is on average displaced by ≈0.2 Å from the rock-salt lattice position, creating a strong phonon scattering mechanism. These findings provide a clue to understanding the excellent thermoelectric performance of crystals with atomic disorder. The SPXRD–MEM approach can be applied in general opening up for widespread characterization of subtle structural features in crystals with unusual properties.

1. Introduction

Thermoelectric materials are functional materials with the unique ability to interconvert heat and electricity,[1] and they show much promise for green energy solutions such as waste heat recovery in automobiles. The thermoelectric figure of merit is defined as $zT = S^2\sigma T/\kappa$, where S is the Seebeck coefficient, σ the electrical conductivity, and κ the thermal conductivity.[1] The extraordinary thermoelectric properties observed for lead chalcogenide (PbX) systems have caused huge research activity,[2–7] and Kanatzidis and co-workers recently reported a breakthrough zT value of 2.2 for nanostructured PbTe,[2] where a strong reduction in κ was achieved without spoiling the power factor, $S^2\sigma$. The lead chalcogenides have remarkable electronic band structures,[4,5] and the electrical properties can be engineered by appropriate chemical doping and substitution. One key issue has been that in bulk PbX crystals, κ is much lower than expected for simple rock-salt structures ($\kappa_{lattice}$(PbX) ≈ 1.5–2.0 W m^{-1} K^{-1} at 300 K).[2] It has been suggested that the low κ is due to a large degree of anharmonicity in the structure, which is supported by first-principles calculations and inelastic neutron scattering (INS) measurements on PbTe.[8–13] The INS studies indicate strong anharmonic coupling between the heat-carrying longitudinal acoustic phonons and the transverse optical phonons.[12,13] Furthermore, pair distribution function analysis showed emerging atomic disorder with temperature, which was coined a "local symmetry broken phase" with "fluctuating dipoles".[14] In simpler terms, this is onset of atomic disorder on the Pb site, where the Pb atom moves away from the (½,½,½) position to the (x,½,½) position. Various studies agree on the off-center displacement of the Pb atom,[8,14] but the literature disagrees on the distance from the rock-salt lattice position and the temperature range of the effect.

In the present study, we probe the atomic disorder in PbTe and PbS based on multi-temperature synchrotron powder X-ray diffraction (SPXRD) data. To date, the studies of the anharmonicity and local disorder have been complex and based on very advanced experimental methods as well as theoretical interpretations. In contrast, SPXRD data can be measured in a few minutes with limited sample preparation. We show that Rietveld refinement, in combination with the latest developments in the maximum entropy method (MEM), can provide very detailed structural information on PbTe and PbS.[15] In diffraction data, the information about atomic disorder and anharmonicity is present in the high-order data, and our study therefore employs SPXRD data measured up to $\sin(\theta)/\lambda = 1.24$ Å^{-1}. Another point is that the MEM uses observed structure factors (F^{obs}) at "face values" without a model to filter out inconsistencies.[16] This means that the accuracy of the data is very important, and systematic errors such as absorption, anomalous scattering, and extinction must be minimized.[17,18] This can be done by measuring SPXRD data on minute samples using high energy radiation, and here we use an X-ray wavelength

Dr. S. Kastbjerg, N. Bindzus, Dr. M. Søndergaard, Dr. S. Johnsen, Dr. N. Lock, Dr. M. Christensen, Prof. B. B. Iversen
Center for Materials Crystallography
Department of Chemistry and iNANO
Aarhus University
Langelandsgade 140, DK-8000 Aarhus C, Denmark
E-mail: bo@chem.au.dk
Prof. M. Takata
Japan Synchrotron Radiation Research Institute
I-I-I, Kouto, Sayo-cho, Sayo-gun, Hyogo 679-5198, Japan
Prof. M. A. Spackman
School of Chemistry and Biochemistry
University of Western Australia
Crawley WA 6009, Australia

DOI: 10.1002/adfm.201300722

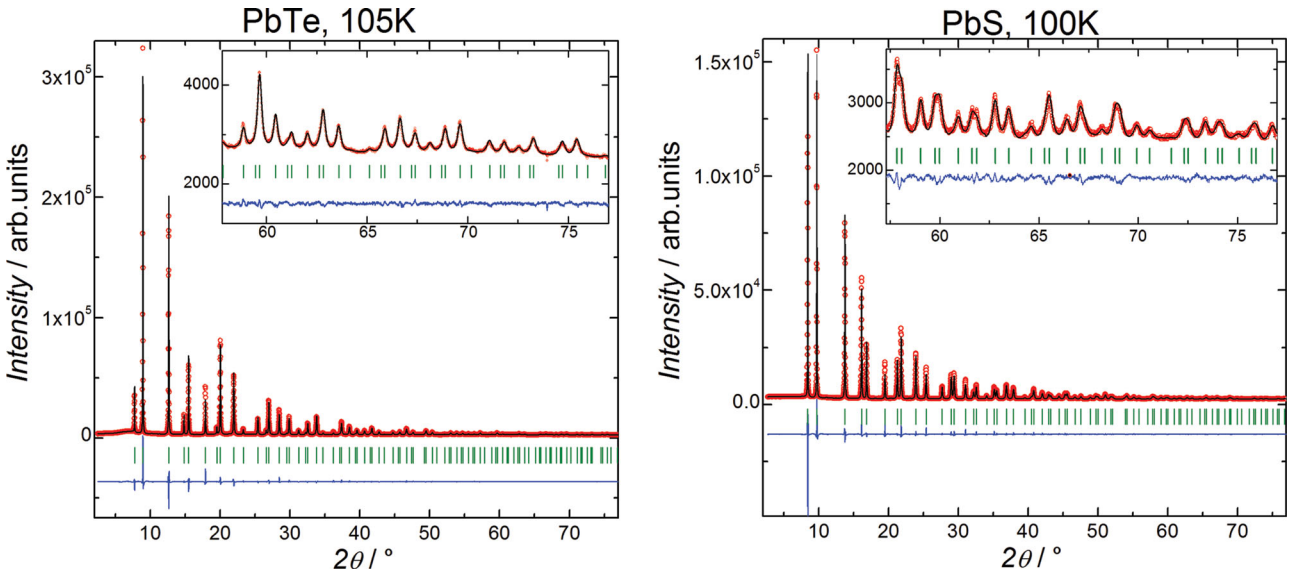

Figure 1. Rietveld refinements of PbTe and PbS data at 105 K and 100 K, respectively, using a harmonic model in the program *FullProf*. Observed (red circles), calculated (black line), and difference (blue line) intensities are shown together with the green markers indicating calculated positions of Bragg peaks for the ideal rock-salt structure. The insets show the high-order data. The agreement factors are R_F(PbTe) = 1.05, R_p(PbTe) = 9.41, R_F(PbS) = 0.95, R_p(PbS) = 10.6.

of 0.500068(2) Å and thin 0.1 mm capillaries. Finally, accurate estimation of the standard deviations of the observed structure factors, $\sigma(F^{obs})$, is critical since i) the basic iterative MEM equation directly contains σ (F^{obs}) in the expression and ii) the MEM stopping criteria for the iterations is based on a χ^2 statistic, which also depends on $\sigma(F^{obs})$.[15] The stopping issue was recently resolved using MEM residual density analysis.[17] Previously, a PXRD–MEM study of PbTe has been reported at room temperature using an in-house diffractometer with wavelength of 1.54 Å and a maximum resolution of $\sin(\theta)/\lambda = 0.56$ Å^{-1}.[19] Despite that those data had much larger absorption than the present data (μ_l = 192.2 mm^{-1} versus 28.2 mm^{-1}), that no residual density analysis was carried out, and that the data had limited resolution in reciprocal space, the corresponding MEM maps still indicated non-spherical electron density features for the Pb atom, demonstrating the power of the MEM in density reconstruction. Subtle details of a density can be enhanced by using difference densities, $\rho^{obs} - \rho^{ref}$, where a well-defined reference density is subtracted from the observed electron density.[20] In crystallography, difference densities are widely used, for instance, to probe bonding features,[21–23] but they can also be used for probing disorder as was, for example, done for guest atoms in thermoelectric clathrates using the MEM.[24,25] In the present study, we use MEM difference densities to visualize and quantify the cation disorder as a function of temperature in PbS and PbTe.

2. Results and Discussion

2.1. Structural Refinements

In **Figure 1**, the 105 K data of PbTe and the 100 K data of PbS are displayed, and the samples are seen to be phase-pure. The lattice parameters of PbTe and PbS at 300 K, 6.46179(3) Å and 5.93293(4) Å, are consistent with the previously reported values.[26]

Figure 2 shows the refined lattice parameters and atomic displacement parameters (ADPs) as functions of temperature, where the heavier Pb atom has a much larger ADP than the lighter Te and S atoms. This can be explained by the disorder around the Pb atom, which is modeled by the ADP. The unit cells show remarkably similar near linear thermal expansion of $2.01(2) \times 10^{-5}$ K^{-1} and $1.98(2) \times 10^{-5}$ K^{-1} at 300 K for PbTe and PbS, respectively, in good agreement with previous studies.[27–29] Since the lead chalcogenides are "simple" structures, the ADPs possibly can be modeled using the Debye expression,[30–32]

$$\langle u^2 \rangle = U_{iso}(T) = \frac{3\hbar^2 T}{m k_B \theta_D^2}\left(\frac{T}{\theta_D}\int_0^{\theta_D/T}\frac{x}{\exp(x)-1}dx + \frac{\theta_D}{4T}\right) + d^2 \quad (1)$$

where θ_D is the Debye temperature, m is the average atomic mass, and d^2 denotes a temperature-independent disorder parameter. The disorder term (somewhat surprisingly) refines to values close to zero. A low Debye temperature (i.e., a large $U_{iso}(T)$ slope) signifies a low velocity of sound, and this leads to a low phonon mean free path and, correspondingly, a low lattice thermal conductivity.[33] The fits to the ADPs of PbTe and PbS give Debye temperatures of 87(1) K and 172(1) K, respectively, which in both cases are slightly lower than previously reported values.[29,34] Above θ_D, the ADPs should depend linearly on the temperature but, as observed in Figure 2, the ADPs exceed the linear increase, which indicates anharmonic vibration or structural disorder.

It is commonly assumed that modeling of anharmonicity requires single crystal neutron diffraction data, which exhibit

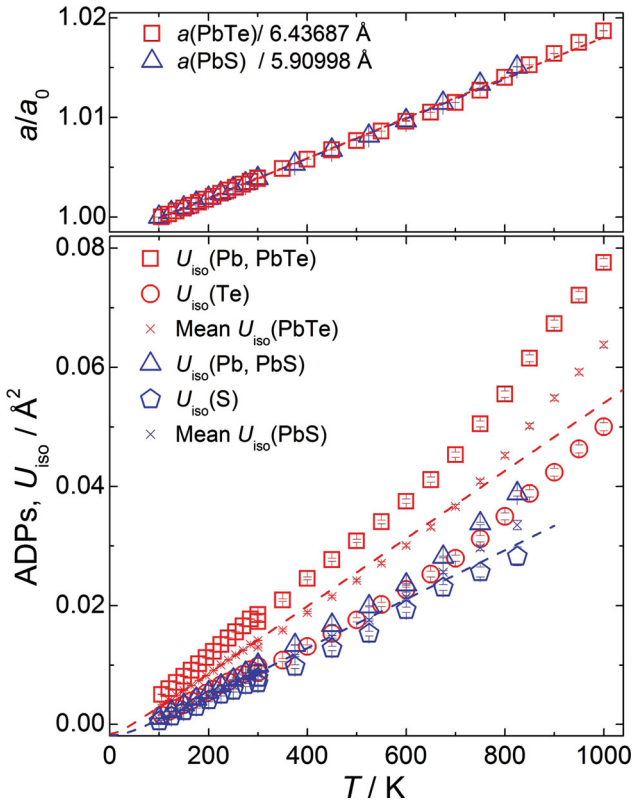

Figure 2. Top: Normalized lattice parameters, *a*, as function of temperature. The dotted lines show the linear fits of the thermal expansions of the cubic unit cells. Bottom: The ADPs of the Pb atoms (red squares and blue triangles), the Te atom (red circles), and the S atom (blue pentagons). All the error bars are smaller than the symbols used. The crosses show the mean ADPs for PbTe (red) and PbS (blue), respectively. The dashed lines correspond to fits of the Debye expression (see text).

no interfering effects of the electron distribution.[20,35] However, recently, the Rietveld refinement program *JANA2006*[36] has been expanded to include anharmonic parameters in form of the Gram-Charlier (GC) expansion of the harmonic termperature factor (see Supporting Information for details).[37] Robust refinement of both multipole electron density parameters and anharmonic GC parameters have been reported for diamond based on SPXRD data,[38] and here we use data at selected temperatures for Rietveld refinement in *JANA2006* with anharmonic ADPs up to fourth order. The anharmonic refinements are stable, and the probability density functions (p.d.f.) in direct space corresponding to the refined GC parameters are plotted in **Figure 3**. Very clear deviations from a Gaussian nuclear p.d.f. are observed for the Pb atom in PbTe and PbS along the axes directions presumably reflecting either anharmonic motion or cation disorder. If these non-Gaussian features are truly vibrational in nature, then we expect the p.d.f. of the Pb atom to be greater in the direction of the empty tetrahedral sites in the rock-salt structure, where the potential is expected to be softer, rather than towards the neighboring atoms.[39] This suggests that the modeled p.d.f. reflects both anharmonic motion and structural disorder, but it should be noted that Bragg diffraction data cannot clearly distinguish between the two. Qualitatively, there is a difference between the PbTe and PbS anharmonic refinements since for PbTe the maximum in the p.d.f. is always found in the lattice position (½,½,½), whereas in PbS it is moved along the axes. The Gram-Charlier parameters model the combined effects of static disorder and anharmonicity, but the latter is expected to be small at low temperature. The low temperature p.d.f. plots therefore strongly suggest that even at ≈100 K there is significant disorder on the Pb site in PbTe and PbS. It is noteworthy that at low temperature the p.d.f. of the lead atom in PbS has unphysical negative features. This presumably reflects that in the modeling of the present data anharmonic/disorder features cannot be adequately deconvoluted from the thermally smeared electron density.

2.2. MEM Analysis

In order to further visualize the cation disorder, MEM calculations were carried out on observed structure factors extracted from the SPXRD data. In peak overlap regions the observed intensity is divided among participating reflections according to the ratio of the calculated structure factors. Consequently, in cases with peak overlap the specific model used to exctract the structure factors will bias the values. It is possible to calculate MEM maps with reduced model bias by treating overlapping reflections as group intensities and implementing them through the so-called G-constraint,[15] which was done using a harmonic model (see Supporting Information). However, it has been shown that improvements in the structural model, results in better structure factor extraction, and thereby superior MEM reconstruction.[17,38] Since both theoretical calculations,[10,11] and experimental data (INS[12,13] and total X-ray scattering[14]) have demonstrated that there is strong atomic disorder and anharmonicity in PbTe, the results shown below are based on the anharmonic Rietveld refinement for extraction of structure factors. However, as shown in the Suppoting Information, the features of the Pb atom obtained with anharmonic structure factor extraction are similar to those based on calculations with a harmonic model and use of G-constraints. The MEM densities were calculated using the Sakata-Sato formalism implemented in *BayMEM*.[15,40] The unit cell was divided into 128 × 128 × 128 pixels and a uniform prior density was used. Use of non-uniform prior densities, for example, in the form of the spherical independent atom model (IAM) of the Rietveld refinement, will typically improve the MEM density.[17] However, here we use uniform prior densities to avoid unnecessary bias about the cation features. Nevertheless, the use of non-uniform priors was tested, and the results are virtually identical to the results reported below (see the Supporting Information). To find the best χ^2 aim values for convergence in the MEM calculations, residual density analysis was carried out, and thus for each temperature the χ^2 aim value resulting in the most Gaussian residual density was chosen (see Supporting Information for details).[17] In **Figure 4**, isosurface plots of the MEM densities are shown at 105 K for PbTe and PbS. The shape of the Pb MEM electron densities are highly distorted reflecting the strong disorder and/or anharmonicity even at 105 K. On the other hand, both the Te and the S atoms appear to be centered on the expected lattice positions. The theoretical calculations by

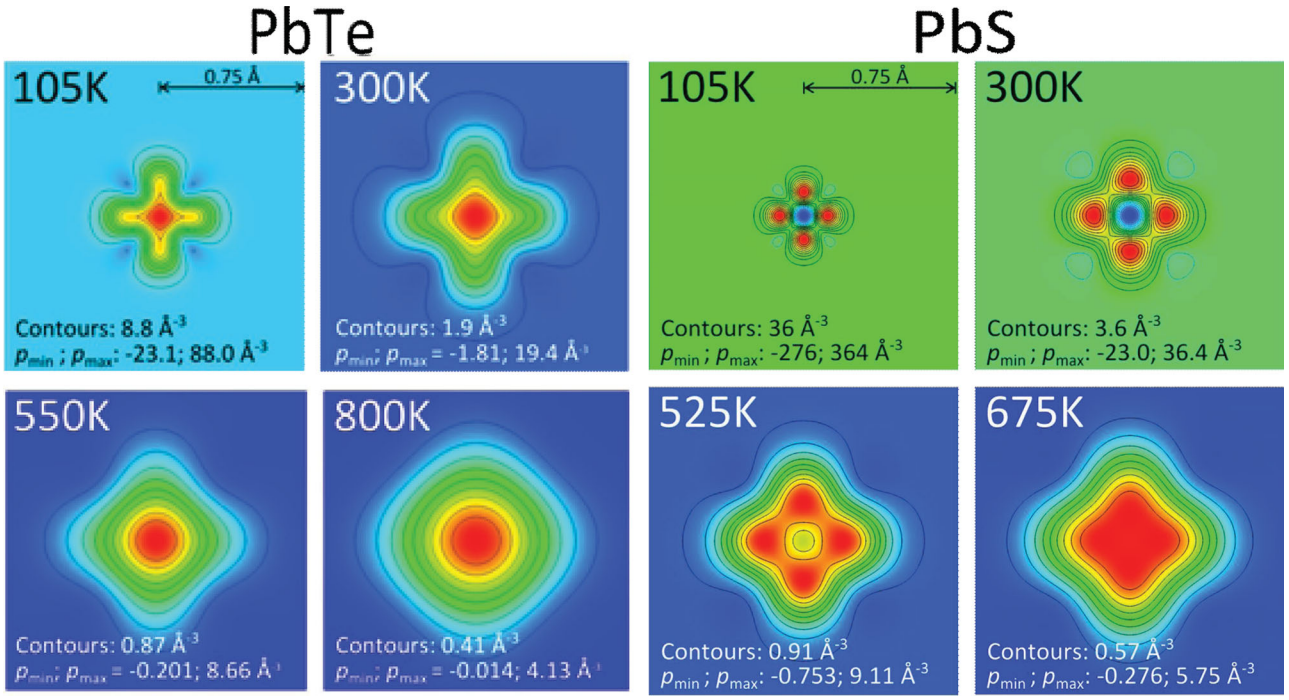

Figure 3. Probability density functions (p.d.f) in the (100) plane through the Pb atom in (½,½,½) obtained from anharmonic refinements of the SPXRD data using *JANA2006*.[36] The plots to the left show the p.d.f. for PbTe and the plots to the right show PbS. Red and blue indicates the maximum and minimum density, respectively, and the temperature dependent contour levels are $p_{max}/10$ with p_{max} indicated on the individual plots.

Kim et al. also predict off-site disorder on the Te site in PbTe, but this is not supported by the present MEM calculations.[11]

Contour plots of the multi-temperature MEM electron densities, ρ^{MEM}, are shown in **Figure 5**, where the distinct non-spherical features are clearly observed for the Pb atom in the form of additional density pointing towards the six Te/S neighbors. In order to emphasize the fine details, MEM difference density maps were calculated by subtracting an IAM density from the observed MEM density. The difference densities, $\rho^{MEM} - \rho^{IAM}$, in Figure 5, show clear maxima for the Pb atoms along the axes directions at all temperatures in both PbTe and PbS, strongly indicating offsets in the Pb atomic positions. On the other hand, the difference density is flatter for Te and S, reflecting a more spherical and structurally ordered nature.

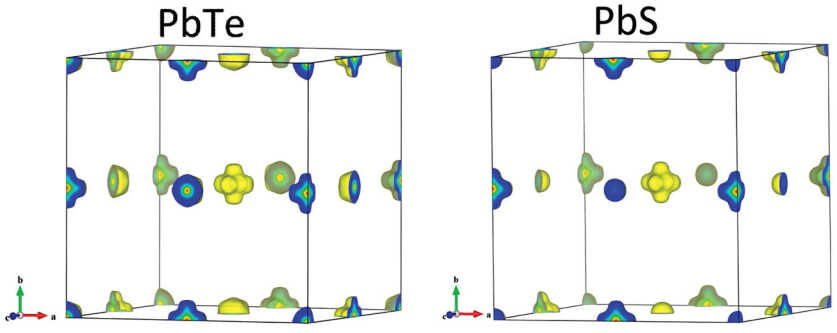

Figure 4. 3D isosurface MEM electron density plots at 105 K of PbTe (left) and PbS (right), respectively. For PbTe the isosurface is at 22 e Å^{-3} and for PbS it is at 30.4 e Å^{-3}.

The temperature dependence of the Pb offset position is plotted in **Figure 6** for comparison with previous studies.[11,14] For PbTe, there is good agreement between the present MEM results and the first-principles calculations by Kim et al.,[11] but the total scattering study by Billinge and co-workers deviates from these, especially at lower temperatures.[14] According to the present MEM study the disorder exists already at 105 K, which is also corroborated by the INS data.[13] The PbS structure has slightly less cation disorder and at 105 K Pb is displaced 0.19 Å compared with 0.25 Å in PbTe. It is important to note that the MEM electron density represents a space–time average picture of the superimposed effects of anharmonic motion and cation disorder. Since anharmonicity is expected to be very strong at high temperature, the exact values of the Pb offset become increasingly uncertain at higher temperature. Nevertheless, in agreement with the previous experimental results, it appears that the cation moves further away from the rock-salt lattice position with increasing temperature. The similar values of the lattice expansion (Figure 2) between PbS and PbTe, as well as the comparable cation disorder, provide a reasonable explanation for their similar values of $\kappa_{lattice}$. If one compares the lattice thermal conductivity to other rock salt structures, then light atom monovalent structures such as NaCl and KBr, which presumably are fully ordered, have room temperature thermal conductivities of

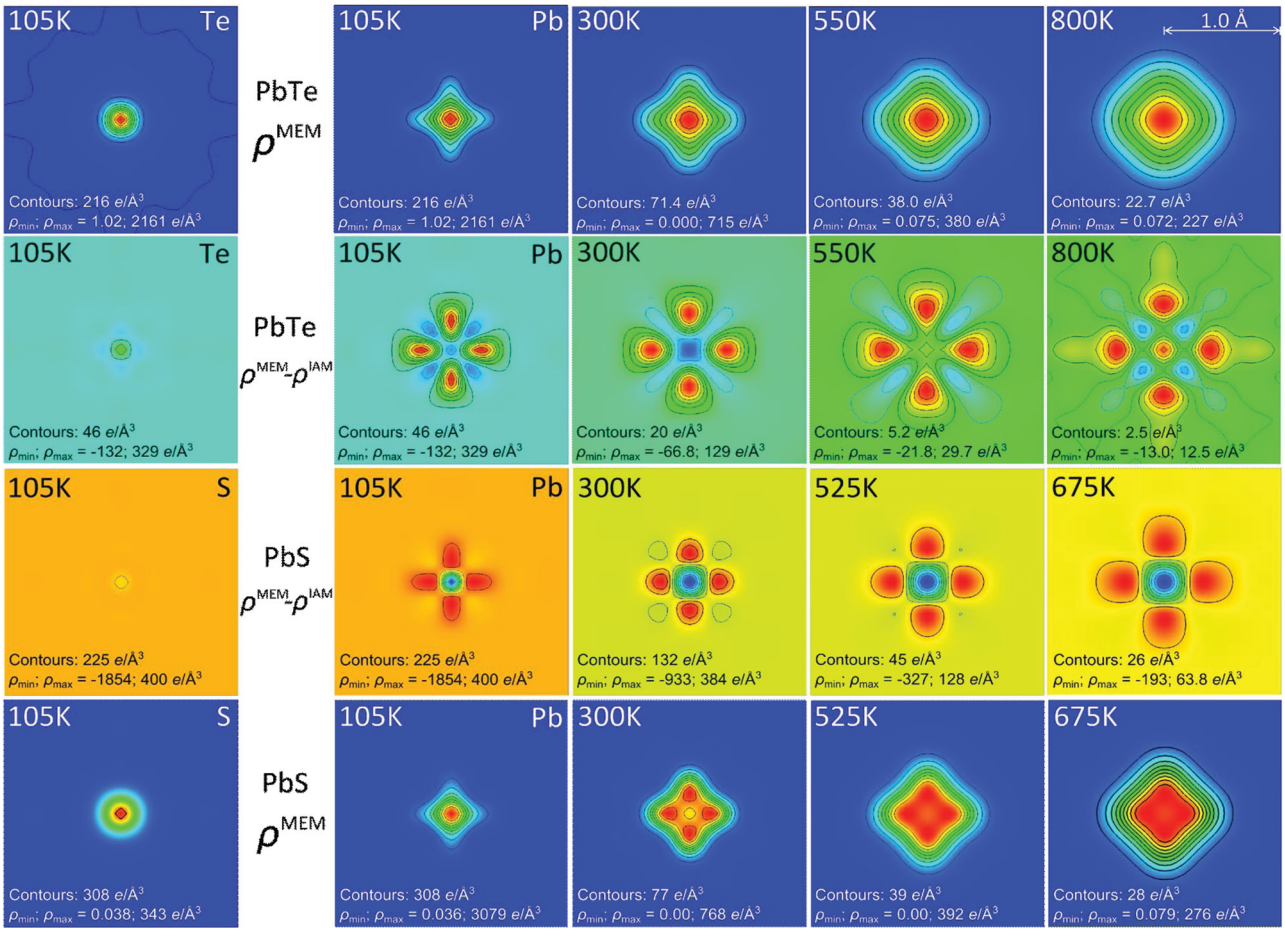

Figure 5. Electron densities obtained through MEM calculations. The plots show 2Å × 2Å of the (100) plane around the Te/S site (0,0,0) or the Pb atom at (½,½,½). Blue and red indicate minimum and maximum density values, respectively. The temperature, scale, and contour levels are listed in the individual plots. First row: electron density ρ^{MEM} of PbTe. Second row: difference density ($\rho^{MEM} - \rho^{IAM}$) of PbTe. Third row: difference density (ρ^{MEM}–ρ^{IAM}) of PbS. Fourth row: electron density ρ^{MEM} of PbS.

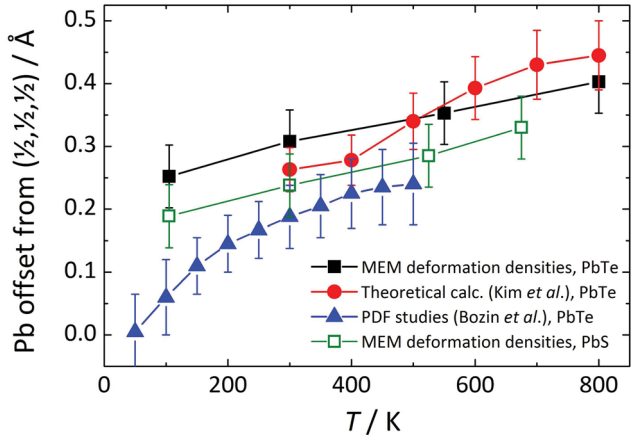

Figure 6. The Pb displacement from (½,½,½) as a function of temperature. The black filled squares and green open squares represent the offset extracted from the MEM difference densities of PbTe and PbS, respectively. Uncertainties are estimated from the grid size of the MEM calculations. The red circles and blue triangles represent previously published results from theoretical calculations and total scattering, respectively.[11,14]

≈6 W K^{-1} m^{-1} and 5 W K^{-1} m^{-1}, respectively.[41] Assuming that phonon–phonon scattering is relatively limited at room temperature, then this could indicate that the cation disorder in PbTe and PbS is a major contributor to lowering the thermal conductivity. However, in these structures, the lighter atomic mass and smaller mass difference between the atoms can also account for their higher thermal conductivity. A rock-salt structure such as AgCl has a very low thermal conductivity of ≈1 W K^{-1} m^{-1},[41] but in this structure, the ionic conductivity (extreme "cation disorder") is large. In some sense, PbTe and PbS represent intermediate structures between fully ordered lattices and ionic conductors. In order to better pinpoint the effect of the disorder on the thermal conductivity, it is clearly of interest to investigate other rock- salt structures using the methods presented here for PbTe and PbS, and such studies are in progress.

It is of interest to quantify and contrast the ionic character of the anions and cations in lead chalcogenides, and this can in principle be done by analyzing the MEM electron densities using the topological methods developed by Bader.[42–44] However, when integrating the charge within the atomic basin retrieved from the zero-flux boundary condition, only

about 72 electrons are retrieved for Pb in PbTe and PbS, while Te has ≈44 electrons and S has ≈10 electrons. The lack of electrons in the atomic basins is due to spurious noise features, which create non-nuclear maxima in the MEM densities that spoil proper characterization of the atomic surfaces. If we, on the other hand, simply divide the unit cell into equal cubes centered on the lattice positions, then charge integration gives +1.14 and +1.11 for Pb in PbTe and PbS, respectively, and corresponding negative charges for Te and S. However, such charge estimates neglect the increase in the atomic volumes of the anions (and decrease of the cation volumes) relative to neutral atoms, and thus the ionic charges presumably are higher. Spherical integration around the lattice positions using the same radius as in the cubes ($a/4$) gives +4.9 for Pb in PbTe and +3.9 for Pb in PbS. The differences between the cube and sphere integrations reflect that significant electron density is present in the interstitial positions in the MEM electron densities.

3. Conclusions

High-resolution and high-energy SPXRD data have been used to visualize and quantify cation disorder in thermoelectric PbTe and PbS. While INS and total scattering data certainly have provided key information about the disorder, the present study shows that crystallographic analysis can provide detailed disorder information from data measured in short time with little sample preparation. The present data suggest that significant cation disorder (≈0.2 Å) is present already at 105 K in both PbTe and PbS. The MEM difference density method can be applied to a wide range of materials, which makes it possible in general to discover structural peculiarities in materials exhibiting unexpected physical properties. It is also very encouraging that the present study shows that anharmonic Gram-Charlier refinements of SPXRD data appear to be robust.

4. Experimental Section

Sample Preparation: Powder samples of PbTe and PbS were prepared in evacuated carbon coated quartz ampoules where stoichiometric mixtures of the elements were melted by heating to 1050 °C and 1100 °C, respectively, which were then slowly cooled. To ensure a homogeneous particle size, the finely ground powder sample was floated in ethanol and left for sedimentation for 30 s before the particles still suspended in ethanol was transferred to another container. This procedure was repeated several times and then the ethanol was evaporated leaving a homogenous fine-grained sample fraction. The powders were transferred to 0.1 mm quartz capillaries and placed in an ultrasound bath for an hour to obtain a dense packing of the powder.

Data Collection: High-resolution multi-temperature SPXRD data were collected on PbTe and PbS with homogenized particle size at beamline BL44B2, SPring8, Japan, using an imaging plate detector.[45] The X-ray wavelength was determined using a CeO_2 standard (a = 5.411102 Å) and well-resolved data were obtained up to $\sin(\theta)/\lambda$ = 1.24 Å^{-1} (7454 data points covering 144 reflections for PbTe, and 7435 data points covering 118 reflections for PbS). The SPXRD data were first Rietveld refined at all temperatures with the *FullProf* program package in the cubic *Fm-3m* space group with full site occupancy in the simple rock-salt structure and a pseudo-Voigt peak shape (X, U, W parameters for low temperatures, but only X and U parameters for high temperatures).[46] The background was refined by linear interpolation between ≈85 points and absorption corrections were performed with μr(PbTe) = 0.70 and μr(PbS) = 0.79 (50% packing density assumed). Due to symmetry restrictions, the ADPs were modeled isotropically (harmonic approximation). Details from the Rietveld refinements of PbTe (105–1000 K) and PbS (100–825 K) are listed in the Supporting Information.

Data Analysis: Data at selected temperatures were also Rietveld refined in *JANA2006*, in which the anharmonicity of the ADPs can be refined using Gram-Charlier coefficients.[36,37] The refinements were again done with a pseudo-Voigt peak shape, but using a 12-term Chebyshev polynomial background and anharmonic Gram-Charlier coefficients to 4th order for the Pb atom. Due to symmetry, the Gram-Charlier coefficients are constrained to be D1111 = D2222 = D3333 and D1122 = D1133 = D2233, while the remaining coefficients are zero. The refined coefficients are listed in the Supporting Information, and since they are not vibrational amplitudes, but terms in a mathematical expansion, they may be negative.

From the anharmonic refinements 144 observed structure factors for PbTe (F^{obs}, 105 K, 300 K) and 118 observed structure factors for PbS (F^{obs}, 105 K, 300 K) were extracted for MEM analysis using the Sakata-Sato formalism implemented in BayMEM.[47] Above room temperature the data sets contained 149 structure factors for PbTe and 121 for PbS. The unit cell was divided into 128 × 128 × 128 pixels and a uniform prior was chosen as initial electron density. To find the best aim values for convergence in the MEM calculations, residual density analysis was carried out following the procedures developed by Bindzus and Iversen.[17] Thus, for each temperature, the MEM calculations were performed to a range of aim values, and after convergence to a given χ^2-aim value, MEM residual densities were computed by inverse Fourier transformation of $F^{obs}(\mathbf{H}) - F^{MEM}(\mathbf{H})$ for each reciprocal lattice vector, $\mathbf{H}$. The optimum χ^2-aim value was chosen as the value where the residual density has the most parabolic fractal dimension distribution.[48] For PbTe the aim values were 1.2, 1.2, 1.0, and 0.8 at 105 K, 300 K, 550 K, and 800 K respectively, while they for PbS were 1.55, 1.8, 1.0, and 3.5 at 105 K, 300 K, 525 K, and 675 K, respectively. All density maps were visualized in *VESTA*.[49]

Supporting Information

Supporting Information is available from the Wiley Online Library or from the author.

Acknowledgements

The work was supported in part by the Danish National Research Foundation (Center for Materials Crystallography, DNRF93). The authors gratefully acknowledge the RIKEN-Harima Institute for beam time at BL44B2 at the SPring8 synchrotron facility.

Received: February 27, 2013
Revised: April 30, 2013
Published online: June 17, 2013

[1] G. J. Snyder, E. S. Toberer, *Nat. Mater.* **2008**, *7*, 105.
[2] K. Biswas, J. He, I. D. Blum, C. I. Wu, T. P. Hogan, D. N. Seidman, V. P. Dravid, M. G. Kanatzidis, *Nature* **2012**, *489*, 414.
[3] J. R. Sootsman, H. Kong, C. Uher, J. J. D'Angelo, C. Wu, T. P. Hogan, T. Caillat, M. G. Kanatzidis, *Angew. Chem., Int. Ed.* **2008**, *47*, 8618.
[4] J. P. Heremans, V. Jovovic, E. S. Toberer, A. Saramat, K. Kurosaki, A. Charoenphakdee, S. Yamanaka, G. J. Snyder, *Science* **2008**, *321*, 554.
[5] Y. Z. Pei, X. Y. Shi, A. LaLonde, H. Wang, L. D. Chen, G. J. Snyder, *Nature* **2011**, *473*, 66.

[6] K. Biswas, J. Q. He, G. Y. Wang, S. H. Lo, C. Uher, V. P. Dravid, M. G. Kanatzidis, *Energy Environ. Sci.* **2011**, *4*, 4675.
[7] Y. Z. Pei, A. LaLonde, S. Iwanaga, G. J. Snyder, *Energy Environ. Sci.* **2011**, *4*, 2085.
[8] Y. Zhang, X. Ke, C. Chen, J. Yang, P. R. C. Kent, *Phys. Rev. B* **2009**, *80*, 024304.
[9] J. An, A. Subedi, D. J. Singh, *Solid State Commun.* **2008**, *148*, 417.
[10] T. Shiga, J. Shiomi, J. Ma, O. Delaire, T. Radzynski, A. Lusakowski, K. Esfarjani, G. Chen, *Phys. Rev. B* **2012**, *85*, 155203.
[11] H. Kim, M. Kaviany, *Phys. Rev. B* **2012**, *86*, 045213.
[12] O. Delaire, J. Ma, K. Marty, A. F. May, M. A. McGuire, M. H. Du, D. J. Singh, A. Podlesnyak, G. Ehlers, M. D. Lumsden, B. C. Sales, *Nat. Mater.* **2011**, *10*, 614.
[13] K. M. O. Jensen, E. S. Bozin, C. D. Malliakas, M. B. Stone, M. D. Lumsden, M. G. Kanatzidis, S. M. Shapiro, S. J. L. Billinge, *Phys. Rev. B* **2012**, *86*, 085313.
[14] E. S. Bozin, C. D. Malliakas, P. Souvatzis, T. Proffen, N. A. Spaldin, M. G. Kanatzidis, S. J. L. Billinge, *Science* **2010**, *330*, 1660.
[15] M. Sakata, M. Sato. *Acta Crystallogr., Sect. A* **1990**, *46*, 263.
[16] B. B. Iversen, F. K. Larsen, M. Souhassou, M. Takata, *Acta Crystallogr., Sect. B* **1995**, *51*, 580.
[17] N. Bindzus, B. B. Iversen, *Acta Crystallogr., Sect. A* **2012**, *68*, 750.
[18] B. B. Iversen, F. K. Larsen, B. N. Figgis, P. A. Reynolds, A. J. Schultz, *Acta Crystallogr., Sect. B* **1996**, *52*, 923.
[19] R. Saravanan, M. C. Robert, *J. Phys. Chem. Solids* **2009**, *70*, 159.
[20] P. Coppens, *X-ray Charge Densities and Chemical Bonding*, Oxford University Press, New York **1997**.
[21] B. B. Iversen, F. K. Larsen, B. N. Figgis, P. A. Reynolds, *Dalton Trans.* **1997**, *13*, 2227.
[22] J. Overgaard, F. K. Larsen, B. Schøtt, B. B. Iversen, *J. Am. Chem Soc.* **2003**, *125*, 11088.
[23] P. Macchi, F. K. Larsen, A. Schultz, B. B. Iversen, *J. Phys. Chem. A* **2001**, *105*, 9231.
[24] A. Bentien, A. E. C. Palmqvist, J. D. Bryan, S. Latturner, G. D. Stucky, L. Furenlid, B. B. Iversen, *Angew. Chem. Int. Ed.* **2000**, *39*, 3613.
[25] C. Gatti, L. Bertini, N. Blake, B. B. Iversen, *Chem. Eur. J.* **2003**, *9*, 4556.
[26] R. Dalven, *Infrared Phys.* **1969**, *9*, 141.
[27] B. Houston, R. E. Strakna, H. S. Belson, *J. Appl. Phys.* **1968**, *39*, 3913.
[28] Z. H. Dughaish, *Physica B* **2002**, *322*, 205.
[29] C. Ghezzi, *Phys. Status Solidi B* **1973**, *58*, 737.
[30] B. T. M. Willis, A. W. Pryor, *Thermal Vibrations in Crystallography*, Cambridge University Press, London **1975**.
[31] A. Bentien, E. Nishibori, S. Paschen, B. B. Iversen, *Phys. Rev. B.* **2005**, *71*, 144107.
[32] J. L. Mi, M. Christensen, E. Nishibori, B. B. Iversen, *Phys. Rev. B* **2011**, *84*, 064114.
[33] N. W. Ashcroft, N. D. Mermin, *Solid State Physics*; Holt, Rinehart and Winston, New York **1976**.
[34] M. Cardona, R. K. Kremer, R. Lauck, G. Siegle, J. Serrano, A. H. Romero, *Phys. Rev. B* **2007**, *76*, 075211.
[35] A. Bentien, B. B. Iversen, J. D. Bryan, G. D. Stucky, A. E. C. Palmqvist, A. J. Schultz, W. Henning, *J. Appl Phys.* **2002**, *91*, 5694.
[36] V. Petricek, M. Dusek, L. Palatinus, *JANA2006 The crystallographic computing system*, Institute of Physics, Praha, Czech Republic **2006**
[37] W. F. Kuhs, *Acta Crystallogr., Sect. A* **1992**, *48*, 80.
[38] H. Svendsen, J. Overgaard, R. Busselez, B. Arnaud, P. Rabiller, A. Kurita, E. Nishibori, M. Sakata, M. Takata, B. B. Iversen, *Acta Crystallogr., Sect. A* **2010**, *66*, 458.
[39] B. B. Iversen, S. K. Nielsen, F. K. Larsen, *Philos. Mag. A* **1995**, *72*, 1357.
[40] S. van Smaalen, J. Netzel, *Phys. Scr.* **2009**, *79*, 048304.
[41] K. A. McCarthy, S. S. Ballard, *J. Appl. Phys.* **1960**, *31*, 1410.
[42] R. F. W. Bader, *Atoms in Molecules: A Quantum Theory*; Oxford University Press, New York **1990**.
[43] L. Palatinus, S. J. Prathapa, S. van Smaalen, *J. Appl. Crystallogr.* **2012**, *45*, 575.
[44] J. Netzel, S. van Smaalen, *Acta Crystallogr., Sect. B* **2009**, *65*, 624.
[45] E. Nishibori, M. Takata, K. Kato, M. Sakata, Y. Kubota, S. Aoyagi, Y. Kuroiwa, M. Yamakata, N. Ikeda, *J. Phys. Chem. Solids* **2001**, *62*, 2095.
[46] J. Rodriguez-Carvajal, *Phys. Rev. B* **1993**, *192*, 55.
[47] S. van Smaalen, L. Palatinus, M. Schneider, *Acta Crystallogr., Sect. A* **2003**, *59*, 459.
[48] K. Meindl, J. Henn, *Acta Crystallogr., Sect. A* **2008**, *64*, 404.
[49] K. Momma, F. Izumi, *J. Appl. Crystallogr.* **2008**, *41*, 653.